J. Fluid Mech. (1998), *vol.* 356, *pp.* 65–91. Printed in the United Kingdom

On the acoustic levitation of droplets

By A. L. YARIN[1], M. PFAFFENLEHNER[2] AND C. TROPEA[2]

[1] Faculty of Mechanical Engineering, Technion – Israel Institute of Technology, Haifa 32000, Israel

[2] Lehrstuhl für Strömungsmechanik, Friedrich–Alexander Universität Erlangen–Nürnberg, Erlangen D-91058, Germany

(Received 4 March 1996 and in revised form 25 March 1997)

This paper deals with the theoretical and experimental investigation of acoustically levitated droplets. A method of calculation of the acoustic radiation pressure based on the boundary element method (BEM) is presented. It is applied to predict shapes of droplets levitated in an acoustic field (and as a result, deformed by it). The method was compared with several known exact and approximate analytical results for rigid spheres and shown to be accurate (and a widely used approximate formula for the acoustic levitation force acting on a rigid sphere was found to be inaccurate for sound wavelengths comparable with the sphere radius). The method was also compared with some other theoretical approaches known from the literature.

Displacement of the droplet centre relative to the pressure node is accounted for and shown to be significant. The results for droplet shapes and displacements are compared with experimental data, and the agreement is found to be rather good. Furthermore, the experimental investigations reveal a unique relationship between the aspect ratio of an oblate droplet and the sound pressure level in the levitator. This relationship agrees well with the predicted shapes. A practical link between droplet shape or droplet displacement and sound pressure level in a levitator is therefore now available.

1. Introduction

Calculations of drop shapes date back to the works of Rayleigh (1879) and Lamb (Lamb 1959, §§275 and 355). Rayleigh gave a linearized solution for small oscillations of an inviscid droplet about its unperturbed spherical shape, whereas Lamb accounted for the effect of small viscosity. Further work on small oscillations of drops accounted for the effects of an arbitrary viscosity (Reid 1960) and passive outer medium (Miller & Scriven 1968; Marston 1980; Prosperetti 1980).

Nonlinear oscillations of inviscid irrotational free drops of moderate amplitude were tackled by perturbation methods in Tsamopoulos & Brown (1983). Studies of arbitrary nonlinear oscillations of drops involve sophisticated numerical methods: boundary integral methods for inviscid irrotational drops (Lundgren & Mansour 1988; Pelekasis, Tsamopoulos & Manolis 1991), and the finite element method for viscous ones (Basaran 1992). Some approximate numerical models of nonlinear drop oscillations were proposed in Becker, Hiller & Kowalewski (1991, 1994). For highly viscous liquids (like those emerging in viscous sintering) the creeping flow approximation is valid. At present the theories of linear and nonlinear droplet oscillations describe satisfactorily most of the experimental findings of Marston & Apfel (1979, 1980), Trinh, Zwern & Wang (1982), Trinh & Wang (1982), and Becker, Hiller & Kowalewski (1991, 1994).

Calculation of shapes of acoustically levitated droplets should account for the detailed structure of the acoustic field around them. This field is governed by the wave

equation (in the linear acoustic approximation). Therefore, calculation of the acoustic field scattered from the drop is reduced to a solution of the Helmholtz equation. The latter may be represented in the form of the boundary integral equation (Lamb 1959, §290; Tikhonov & Samarskii 1990, Chapter 7, §2.2). Thus calculation of the scattered field and the force imposed on a droplet by the acoustic field may be performed using a numerical implementation of the boundary integral equation. In parallel, the steady-state shape of the droplet or its evolution may be found by solving either ordinary differential equations governing the force balance at the surface or the boundary integral equation of the theory of potential (Jaswon & Symm 1977; Becker 1992) for inviscid irrotational flow inside the droplet. Several examples of this approach have already appeared in the literature. Lee, Anilkumar & Wang (1994) calculated the static shape of a droplet located forcedly at the pressure node of a standing acoustic wave, whereas Shi & Apfel (1995*a*, *b*) calculated small oscillations of an acoustically deformed drop, as well as droplet squeezing in a strong acoustic field. Using artificial damping of droplet oscillations, Shi & Apfel (1996) applied their method to predict steady deformation and the position of acoustically levitated droplets. Their results were published when the present work was in press. It is worth mentioning that several approximate theories of steady droplet shapes in acoustic fields, valid in a restricted aspect ratio range (not very large), have been published, e.g. Marston (1980) and Tian, Holt & Apfel (1993).

The aim of the theoretical part of the present work is the prediction of steady-state shapes of droplets levitated acoustically, and comparison of theoretical results with experimental data. The theoretical work includes development of a novel method based on the boundary integral equation, as well as a comparison of the whole droplet shape and its displacement relative to the pressure node with experimental data. The method directly solves a steady problem.

Experimental investigations of levitated droplets have been performed by Lierke (1996), who gave an extensive overview on acoustic levitation and the effects of the acoustic field on droplet physics. Also, Daidzic (1995) investigated several effects of acoustically levitated droplets but, like Trinh & Wang (1982), mainly concentrated on droplet oscillations. Trinh & Hsu (1986), Lee, Anilkumar & Wang (1991) and Anilkumar, Lee & Wang (1993*b*) visualized the shapes of droplets deformed by the acoustic field up to the point of droplet breakup. The bifurcation of rotating droplets under microgravity condition was investigated by Anilkumar, Lee & Lin (1993*a*).

One major obstacle in analysing experimental results is knowing reliably the sound pressure level (SPL) in the levitator. In principle, one could use a microphone; however, the acoustic field is sensitive to such intrusions. Although the calibration of the levitator is of central importance, few papers address this issue explicitly. They mainly deal with sound pressure calibration using small solid spheres or droplets, like for example in Apfel (1971) or in the dropout method also analysed in the present work. However, the presence of a large squeezed drop results in a resonance shift caused by scattering (Trinh & Hsu 1986), which makes results of sound pressure calibration by small spheres or droplets inaccurate. The idea of using droplet deformation to calibrate sound pressure was briefly mentioned in Tian *et al.* (1993), as well as in Shi & Apfel (1996) where the measurement of the deformed shape of a small drop was addressed. One aim of the present experimental work is, therefore, to establish a means of estimating SPL for a given driving voltage of the levitator, a given droplet size (even large) and fluid and a given resonator geometry. As a result, a practical link between droplet deformation and SPL is established.

In §2 we describe the boundary integral method used to calculate the scattered

acoustic field. In §3 we test this method against several known exact and approximate analytical results for rigid spheres. In §4 we present the method used to calculate steady-state droplet shapes in an acoustic field. The experimental set-up is outlined in §5. Also in §5 the results of the calculations are presented and compared with experimental data. This yields a link between driving voltage and SPL. Finally in §5 the results of the calculations are compared with experimental data of Trinh & Hsu (1986) and several theoretical predictions taken from the literature. Conclusions are given in §6.

2. Acoustic field

Acoustic levitators are typically assumed to operate in a regime close to 'resonance' when a standing sound wave of high (but finite) amplitude sets in. This happens when an excitation frequency and eigenfrequency of a levitator become equal. Calculation of the standing wave in a finite-length levitator based on a wave equation evidently yields an infinite amplitude, since dissipative effects, such as viscosity and heat conduction, are neglected. In reality, these effects make the amplitude finite. It is convenient to assume the acoustic field to be a harmonic standing wave of some given amplitude, which corresponds to a solution of the wave equation for an infinitely long levitator. This approach was adopted, for example, in Lee *et al.* (1994) and Shi & Apfel (1995*a*).

Experiments of the present work show that droplets cannot be suspended if the eigenfrequency of the levitator is equal to that of the ultrasound wave, since the amplitude of the latter becomes so high that the droplets become unstable and oscillate. In the present set-up that leads to a rapid droplet shatter. However, by detuning the levitator by varying the reflector distance L_r, a standing wave of lower, but still high enough, amplitude for droplet levitation is obtained. The incident ultrasound wave in the levitator is assumed to be one-dimensional and satisfies the one-dimensional wave equation with appropriate boundary conditions at the source of the sound ($x = 0$) and the reflector ($x = L_r$):

$$\frac{\partial^2 p_i'}{\partial t^2} = c_0^2 \frac{\partial^2 p_i'}{\partial x^2}, \tag{2.1a}$$

$$x = 0: \quad p_i' = A_0 \, \mathrm{e}^{-\mathrm{i}\omega t}, \tag{2.1b}$$

$$x = L_r: \quad \frac{\partial p_i'}{\partial x} = 0, \tag{2.1c}$$

where p_i' is the pressure perturbation in the incident wave, A_0 is its amplitude at the source (piezocrystal) surface, ω is its angular frequency (corresponding to the ultrasonic range), c_0 is the sound velocity in air, i is the imaginary unity, t is time, and x is the longitudinal (vertical) coordinate.

The solution of (2.1) is given by

$$p_i' = A_0 \, \mathrm{e}^{-\mathrm{i}\omega t} \left[\tan\left(\frac{\omega L_r}{c_0}\right) \sin\frac{\omega x}{c_0} + \cos\frac{\omega x}{c_0} \right], \tag{2.2}$$

where $\omega L_r / c_0$ should not be equal $\pi/2 + \pi n$ ($n = 0, 1, 2, \ldots$), since the levitator is to be detuned. This corresponds also to the conditions of the present experiment ($\omega = 2\pi \times 56$ kHz, $c_0 = 3.4 \times 10^4$ cm s^{-1}, $L_r \approx 1.6$ cm). Under these conditions there are five nodes of p_i' inside the levitator, at

$$x = L_r - \frac{c_0}{\omega}\left(\frac{\pi}{2} + \pi n\right), \quad n = 0, 1, 2, 3, 4 \tag{2.3}$$

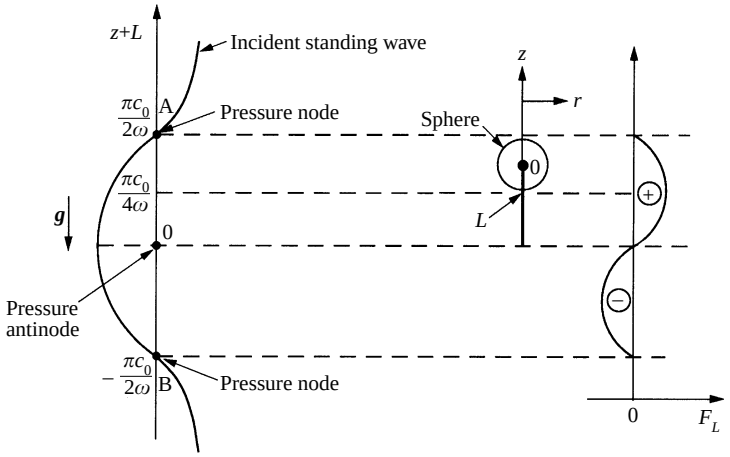

FIGURE 1. Sketch of the incident acoustic wave with the frame of reference. F_L is the acoustic levitation force acting on a rigid sphere.

as well as three maxima and minima at

$$x = L_r - \frac{c_0}{\omega}\pi n \tag{2.4}$$

with $n = 1, 3, 5$ and $n = 0, 2, 4$, respectively. Note that in the present experiment, droplets were levitated near the third node corresponding to $n = 2$ in (2.3).

Similar to Lee *et al.* (1994) and Shi & Apfel (1995*a*) we approximate the incident wave (2.2) by a standing wave corresponding to an infinite levitator:

$$p_i' = A_{0e}\,\mathrm{e}^{-\mathrm{i}\omega t}\cos\frac{\omega}{c_0}x, \tag{2.5}$$

where A_{0e} is an effective amplitude, $x = z + L$, z is the vertical coordinate where $z = 0$ may be considered to be the position of the centre of an imaginary (or real) levitated rigid sphere, and L is the displacement of the centre of this sphere (or the origin of the z-axis) relative to the pressure antinode (see figure 1).

To make the approximation (2.5) consistent with (2.2) we need to require the maxima of p_i' to be identical in both the cases, which yields

$$A_{0e} = -\frac{A_0}{\cos(\omega L_r/c_0)}. \tag{2.6}$$

Under the conditions of the present experiment $\cos(\omega L_r/c_0) = -0.660$ (for $L_r = 1.6$ cm).

The approximation (2.5) and (2.6) yields the amplitude of the sound wave and the number of pressure nodes in $0 \leqslant x \leqslant L_r$ identical with those of (2.2). The displacement of a pressure node given by (2.5) and (2.6) relative to that of (2.2) is about 5% ($\Delta x/L_r \approx 0.05$). In the following we mimic the incident standing wave by (2.5) with the amplitude A_{0e} related to that of the sound source A_0 by (2.6).

When a droplet (or a rigid particle) is located in the levitator, a scattered acoustic field appears in addition to the incident one (2.5):

$$p_s' = A_{0e}\,\mathrm{e}^{-\mathrm{i}\omega t}p_s(\boldsymbol{r}), \tag{2.7}$$

where function p_s of the radius-vector $\boldsymbol{r}$ is to be found from the Helmholtz equation:

$$\Delta p_s + \left(\frac{\omega}{c_0}\right)^2 p_s = 0. \tag{2.8}$$

The effect of the acoustic wave inside the droplet on the shape of the droplet is negligibly small, since fluids of interest have much larger values of acoustic impedance than that of air. Therefore, equation (2.8) is supplemented by the boundary condition expressing the fact that droplets (like rigid particles) are practically impenetrable by sound waves: $\boldsymbol{n}\cdot\boldsymbol{\nabla}(p_i' + p_s') = 0$ at the surface, where $\boldsymbol{n}$ is the unit vector of the outer normal to the surface. This yields the following boundary condition at the surface:

$$\boldsymbol{n}\cdot\boldsymbol{\nabla} p_s = -\boldsymbol{n}\cdot\boldsymbol{\nabla}\left\{\cos\left[\frac{\omega}{c_0}(z+L)\right]\right\}. \tag{2.9}$$

In the case of droplet levitation in a liquid (which is not the aim of the present work) the boundary condition (2.9) should be modified to account for the sound field inside the droplet, e.g. as in Tian *et al.* (1993). Far from the droplet (or particle) the scattered field is supposed to be vanishing:

$$p_s \to 0 \quad \text{as} \quad \boldsymbol{r} \to \infty. \tag{2.10}$$

Solutions of equation (2.8) with boundary conditions (2.9) and (2.10) may be found from the following boundary integral equation (Lamb 1959, §290; Tikhonov & Samarskii 1990, Chap. 7, §2.2):

$$p_s(P) = \frac{1}{2\pi}\int\int_S p_s(Q)\frac{\partial}{\partial n}\left[\frac{\exp(\mathrm{i}\omega r_{PQ}/c_0)}{r_{PQ}}\right]\mathrm{d}\sigma_Q + \frac{1}{2\pi}\int\int_S \frac{\exp(\mathrm{i}\omega r_{PQ}/c_0)}{r_{PQ}}\frac{\partial}{\partial n}\left\{\cos\left[\frac{\omega}{c_0}(z+L)\right]\right\}\mathrm{d}\sigma_Q \tag{2.11}$$

(the Fredholm equation of the second kind).

The integrals in (2.11) are evaluated over the droplet (or particle) surface S. P is a point at the surface where p_s is calculated, whereas Q is any point at the surface. The distance between these points is denoted by r_{PQ}; the element of area is $\mathrm{d}\sigma_Q$.

In the present paper we assume that droplets have only axisymmetric shapes. This assumption is supported by the experimental evidence shown in figure 6 below. For axisymmetric droplets (or particles) equation (2.11) may be rearranged to the following system of boundary integral equations used to find the real and imaginary parts of the scattered wave p_{sr} and p_{si}:

$$\int p_{sr}(Q)\,G_1(P,Q)\,\mathrm{d}s + \int p_{si}(Q)\,H_1(P,Q)\,\mathrm{d}s - p_{sr}(P) = \int M_1(P,Q)\,\mathrm{d}s, \tag{2.12a}$$

$$\int p_{sr}(Q)\,G_2(P,Q)\,\mathrm{d}s + \int p_{si}(Q)\,H_2(P,Q)\,\mathrm{d}s - p_{si}(P) = \int M_2(P,Q)\,\mathrm{d}s. \tag{2.12b}$$

The kernel functions G_i, H_i and M_i $(i = 1, 2)$ are given in the Appendix. In equations (2.12) the integrals are evaluated using an arbitrary parameter of a half-loop of the drop generatrix, s. When applying the boundary element method (BEM) and

discretizing (2.12) on the boundary elements, we take s rendered dismensionless by the unperturbed drop (or particle) radius a_0. Also s varies from $s=-1$ to $s=1$ along an element in the direction from the droplet top to the bottom. Discretization of (2.12) and numerical evaluation of the integrals involved is similar to the procedure described by Becker (1992). The resulting system of algebraic equations

$$\boldsymbol{B}\cdot\begin{bmatrix}\boldsymbol{p}_{sr}\\ \boldsymbol{p}_{si}\end{bmatrix}=\boldsymbol{D} \tag{2.13}$$

is solved by the Gaussian elimination technique. As a result, the column of nodal values of p_{sr} and p_{si} is found for known matrices $\boldsymbol{B}$ and $\boldsymbol{D}$.

The total pressure perturbation at the droplet (or particle) surface is given by the sum

$$p'=p'_i+p'_s, \tag{2.14}$$

where p'_i and p'_s are taken at the surface.

The acoustic radiation pressure is given by (Landau & Lifshitz 1959, §64)

$$p_a=\frac{\langle p'^2\rangle}{2\rho_0 c_0^2}-\frac{\rho_0}{2}\langle \boldsymbol{v}'\cdot\boldsymbol{v}'\rangle, \tag{2.15}$$

where the acoustic gas velocity is

$$\boldsymbol{v}'=\boldsymbol{\nabla}\left(-\frac{1}{\rho_0}\int_0^t p'\,\mathrm{d}t\right) \tag{2.16}$$

and $\langle\ \rangle$ denotes time averaging over a period long enough compared with the wave cycle, and ρ_0 is the unperturbed air density.

Using (2.5), (2.7) and (2.14)–(2.16) we arrive at the acoustic radiation pressure produced by the standing wave at the drop (or particle) surface,

$$p_a=\frac{A_{0e}^2}{4\rho_0 c_0^2}\left\{\left[p_{sr}+\cos\left(\frac{\omega}{c_0}(z+L)\right)\right]^2+p_{si}^2\right\}$$
$$-\frac{A_{0e}^2}{4\rho_0\omega^2}\left\{\left(\frac{1}{\lambda}\frac{\partial p_{si}}{\partial s}\right)^2+\left[\frac{1}{\lambda}\frac{\partial p_{sr}}{\partial s}-\frac{1}{\lambda}\frac{\partial z}{\partial s}\frac{\omega}{c_0}\sin\left(\frac{\omega}{c_0}(z+L)\right)\right]^2\right\}, \tag{2.17}$$

where p_{sr} and p_{si} at the surface are found from (2.13), and the generatrix stretch is

$$\lambda=\left[\left(\frac{\partial r}{\partial s}\right)^2+\left(\frac{\partial z}{\partial s}\right)^2\right]^{1/2}. \tag{2.18}$$

Note that r and z are radial and axial coordinates of a point on the droplet (or particle) generatrix. The overall acoustic force acting on an axisymmetric droplet (or particle) is equal to

$$\boldsymbol{F}=-2\pi\int_{\mathrm{Top}}^{\mathrm{Bottom}} p_a\,\boldsymbol{n}r\lambda\,\mathrm{d}s \tag{2.19}$$

which yields the acoustic levitation force in the form

$$F_L=F_z=-2\pi\int_{\mathrm{Top}}^{\mathrm{Bottom}} p_a\frac{\partial r}{\partial s}r\,\mathrm{d}s, \tag{2.20}$$

where p_a is given by (2.17).

3. Test cases for the acoustic scattering and levitation force calculations

King (1934) solved two important problems of the theory of acoustic scattering, which may be readily used for testing the numerical approach outlined in §2, as well as for a rough estimate of the spatial distribution of the acoustic levitation force acting on a droplet.

In the first example of King (1934) a travelling acoustic pressure wave

$$p_i' = A_{0e}\,\mathrm{e}^{\mathrm{i}k(z-c_0 t)} \tag{3.1}$$

(k is the wavenumber, $k = \omega/c_0$) is scattered from an immovable rigid sphere of radius a_0 with the centre at $z = 0$. His solution for this case is also given in Morse (1948, p. 354) and Tikhonov & Samarskii (1990, Chap. 7, §4.3).

Note that in the numerical calculation of scattering of the travelling wave (3.1) from a sphere (to compare the results with the above analytical solution), only the non-dimensional functions M_1 and M_2 in the Appendix should be changed. They become as follows:

$$M_1(P,Q) = -\frac{2}{\pi}\Omega\frac{\partial r}{\partial s}(-F\cos\Omega z - Y\sin\Omega z)\frac{r}{A^{1/2}}, \tag{3.2a}$$

$$M_2(P,Q) = -\frac{2}{\pi}\Omega\frac{\partial r}{\partial s}(Y\cos\Omega z - F\sin\Omega z)\frac{r}{A^{1/2}} \tag{3.2b}$$

(cf. (A 4e, f)). All the other functions obtained previously for a standing wave remain unchanged.

The results of the calculation of the scattered acoustic field based on the analytical solution of King (1934) were compared with the present numerical results and found to be practically indistinguishable.

The second example given by King (1934) includes calculation of the acoustic levitation force F_L acting on a rigid immovable sphere located in the incident wave (2.5). His analytical result is given by

$$\frac{F_L}{\rho_0 c_0^2 a_0^2} = \pi\left(\frac{A_{0e}}{\rho_0 c_0^2}\right)^2 \sin(2\Omega L) f(\Omega) \tag{3.3}$$

with

$$\Omega = k a_0, \tag{3.4a}$$

$$f(\Omega) = f_{King}(\Omega) = \frac{1}{\Omega^2}\left\{\frac{1}{\Omega}\frac{F_0 F_1 + G_0 G_1}{H_0^2 H_1^2} - \frac{2}{\Omega^5}\frac{(F_1 F_2 + G_1 G_2)}{H_1^2 H_2^2}(\Omega^2 - 3) + \sum_{m=2}^{\infty}(-1)^m \frac{(m+1)}{\Omega^{2m+3}}\frac{(F_{m+1}F_m + G_{m+1}G_m)}{H_m^2 H_{m+1}^2}[\Omega^2 - m(m+2)]\right\}. \tag{3.4b}$$

The argument of the functions F_i, G_i and H_i in (3.4b) is Ω; the functions are defined as

$$F_m(\Omega) = -\Omega^{1-m} n_{m+1}(\Omega) + \frac{m}{\Omega^m} n_m(\Omega), \tag{3.5a}$$

$$G_m(\Omega) = \Omega^{1-m} j_{m+1}(\Omega) - \frac{m}{\Omega^m} j_m(\Omega), \tag{3.5b}$$

$$H_m(\Omega) = [F_m^2(\Omega) + G_m^2(\Omega)]^{1/2}, \tag{3.5c}$$

where j_m and n_m are the spherical Bessel and Neumann functions respectively, and L

L	F_L, numerical	F_L, by (3.3) with (3.4b)	F_L, by (3.3) with (3.6)
0	−0.0096	0	0
0.1	0.2737	0.2840	0.3397
$\frac{1}{4}\pi = 0.785$	1.4148	1.4294	1.7098
1	1.2849	1.2998	1.5547
1.55	0.0466	0.0594	0.0711

TABLE 1. The values of the acoustic levitation force acting on a rigid immovable sphere obtained numerically, and by means of the exact – (3.3) with (3.4b) – and approximate – (3.3) with (3.6) – analytic results. F_L is rendered dimensionless by $\rho_0 c_0^2 a_0^2$, L by a_0. $A_{0e}/\rho_0 c_0^2 = 1$, $\Omega = 1$.

in (3.3) is rendered dimensionless by a_0. Note that according to figure 1, displacement of a rigid sphere from the pressure node rendered dimensionless by a_0, is $D = \pi/2\Omega - L$. Therefore, $\sin(2\Omega L) = \sin(2\Omega D)$ in (3.3).

It is emphasized that the result of King (1934) (3.3)–(3.5) is valid for an arbitrary value of Ω including $\Omega = O(1)$. King (1934) also obtained a simple asymptotic form of (3.3)–(3.5), valid only for $\Omega \ll 1$, which is not considered in the present paper.

An approximate expression for the acoustic levitation force imposed on a rigid immovable sphere by relatively long ultrasonic waves ($\Omega = ka_0 \ll 1$) was proposed in Leung, Jacobi & Wang (1981), Lierke *et al.* (1983) and Lierke (1996). It is given by (3.3) with

$$f(\Omega) = f_{LJW}(\Omega) = \tfrac{5}{6}\Omega \frac{3}{(2\Omega)^2}\left[\frac{\sin(2\Omega)}{2\Omega} - \cos(2\Omega)\right]. \tag{3.6}$$

In table 1 we compare the results obtained numerically by means of (2.13), (2.17) and (2.20) (with 51 nodal points on a half-loop of the generatrix) with those given by (3.3) with (3.4b), and (3.3) with (3.6) for $A_{0e}/\rho_0 c_0^2 = 1$ and $\Omega = 1$. The displacement of the sphere centre relative to the pressure antinode was varied. It is seen that for the acoustic wave of an intermediate length corresponding to $\Omega = 1$, in the most important range of L from $\pi/4$ (where F_L has a maximum according to (3.3)) to 1, the numerical result differs from the exact one, (3.3) with (3.4b), by 1%. The approximate result (3.3) with (3.6) differs from the exact one by 16–19.6%.

The results of the comparison allow us to expect that the numerical calculation of the acoustic levitation force is accurate enough to use this method in the case of non-spherical droplets deformed by the acoustic field also.

4. Steady-state shapes of acoustically levitated droplets

Steady suspension of a droplet in a standing acoustic wave results from an equilibrium of the acoustic levitation and gravity forces:

$$-2\pi \int_{\text{Top}}^{\text{Bottom}} p_a \frac{\partial r}{\partial s} r \, \mathrm{d}s = \tfrac{4}{3}\pi a_0^3 \rho_l g. \tag{4.1}$$

The integral is evaluated over a half-loop of the generatrix, the unperturbed drop radius is denoted a_0, liquid density is ρ_l, and gravity acceleration is g. The acoustic radiation pressure p_a is given by (2.17), and depends on the droplet shape and L.

Against the background of the overall force equilibrium (4.1), a pointwise equilibrium of the acoustic, capillary and hydrostatic pressures may be achieved at the

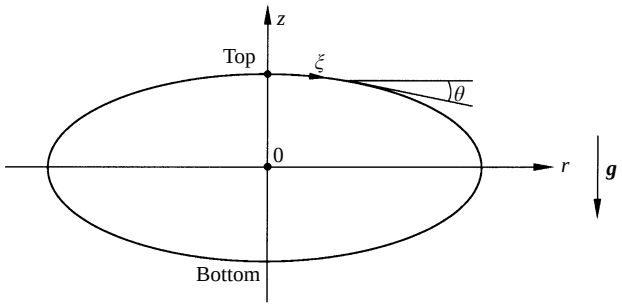

FIGURE 2. Sketch of a squeezed droplet. The tangent slope shown is negative ($\theta < 0$).

droplet surface, resulting in a steady-state shape. The fluid pressure at the droplet surface is given by

$$p = p_0 + p_a - \alpha K, \tag{4.2}$$

where p_0 is an unperturbed air pressure, α is the surface tension coefficient, and K is the surface curvature (negative at a convex surface and positive at a concave one).

Using (4.2) we get from the Bernoulli equation at the droplet surface

$$\frac{p_a}{\rho_l} - \frac{\alpha}{\rho_l} K + gz = C, \tag{4.3}$$

where the constant C includes p_0.

Pressure p_a is rendered dimensionless by $\rho_0 c_0^2$, K by a_0^{-1}, z by the equivalent droplet radius a_0, and C by $\alpha/\rho_l a_0$. Thus, we rearrange (4.3) to the non-dimensional form

$$K - We_a p_a - Bo\, z = -C, \tag{4.4}$$

where the modified acoustic Weber number We_a and Bond number Bo are defined as

$$We_a = \frac{\rho_0 c_0^2 a_0}{\alpha}, \quad Bo = \frac{\rho_l g a_0^2}{\alpha}. \tag{4.5a, b}$$

Defining a tangent slope to the generatrix θ and the arclength from the top ξ (see figure 2) we get the curvature in the following form:

$$K = \frac{\sin\theta}{r} + \frac{\mathrm{d}\theta}{\mathrm{d}\xi}. \tag{4.6}$$

Using (4.6) we obtain from (4.4) and simple geometrical considerations the following equations used to calculate the droplet shape:

$$\frac{\mathrm{d}\theta}{\mathrm{d}\xi} = -C + We_a p_a + Bo\, z - \frac{\sin\theta}{r}, \tag{4.7a}$$

$$\frac{\mathrm{d}r}{\mathrm{d}\xi} = \cos\theta, \tag{4.7b}$$

$$\frac{\mathrm{d}z}{\mathrm{d}\xi} = \sin\theta. \tag{4.7c}$$

It is easy to see that as ξ tends to zero, θ is proportional to ξ, $r = \xi$ and $z = z_T$, where z_T is a coordinate of the droplet top. Therefore, the boundary condition allowing one to avoid the singularity at the top, is posed at some small ξ_0:

$$\xi = \xi_0: \quad \theta = M\xi_0, \quad r = \xi_0, \quad z = z_T, \tag{4.8a–c}$$

with

$$M = \tfrac{1}{2}[-C + We_a p_{aT} + Bo\, z_T], \tag{4.9}$$

where p_{aT} is a value of the acoustic radiation pressure at the top.

The value of C in (4.7a) is found by shooting with the goal of satisfying the condition that at some $\xi = \xi_B$ where $\theta = -\pi$, it should also be the case that

$$r = 0. \tag{4.10}$$

When this condition is reached, ξ_B is identified as an arclength of the half-loop of the droplet generatrix. The shooting method employed in the present work to solve equations (4.7) is close to that of Goldshtik, Khanin & Ligai (1986) where it was proven to be highly effective and flexible in calculations of shapes of droplets levitated by air blowing or due to evaporation above a hot plate (Leidenfrost effect).

The whole algorithm works via iterations as follows.

(i) First we suppose an arbitrary droplet shape defined as functions $r(s)$ and $z(s)$.

(ii) Then we calculate the corresponding volume as

$$V = \int_{z_B}^{z_T} \pi r^2 \, \mathrm{d}z, \tag{4.11}$$

where z_T and z_B are the coordinates of the top and bottom. Using (4.11) we can calculate the factor ζ:

$$\zeta = \left(\frac{4\pi a_0^3}{3V}\right)^{1/3}. \tag{4.12}$$

Given $r(s)$ and $z(s)$ and multiplying them by this factor, we adjust the droplet volume to that of the unperturbed drop (without changing a shape of the former). Note, that the present stage yields a trivial result $\zeta = 1$ for an initial guess in the form of a spherical droplet of radius a_0 used in the calculations.

(iii) Then we suppose a value of the displacement of a coordinate system associated with the centre of an imaginary rigid sphere, L (see figure 1), and calculate the distribution of the acoustic radiation pressure p_a at the droplet surface from (2.13) and (2.17). Then iterating L we try to satisfy the overall force balance (4.1) for the drop, which in the non-dimensional form is written as

$$-\int_{\mathrm{Top}}^{\mathrm{Bottom}} p_a \frac{\partial r}{\partial s} r \, \mathrm{d}s = \frac{2}{3}\frac{Bo}{We_a}. \tag{4.13}$$

Note that the displacement of a drop relative to the pressure antinode is evidently distinct from L: a real droplet may be also displaced relative to the probe imaginary rigid sphere. Droplet displacement relative to the pressure node (and antinode) is discussed below (see (4.14)).

The range of L, $0 \lesssim L \lesssim \pi/2\Omega$ (rendered dimensionless by a_0) where the acoustic levitation force F_L is expected to be positive, is the only one where the iterations in L may converge in the case when droplet suspension may be possible. However, there is

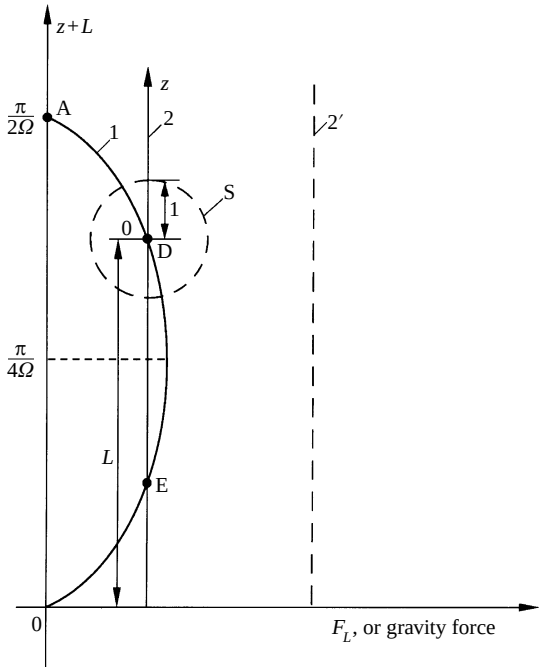

FIGURE 3. The overall force balance. Curve 1 is the acoustic levitation force; vertical lines 2 and 2′ are two different values of the gravity force. An imaginary rigid sphere S is also shown. The origin of the z-axis is associated with its centre. Point A is the pressure node.

a case when it is, in principle, impossible (see figure 3). When the droplet weight is larger than the maximum of F_L (see vertical line 2′ in figure 3), there cannot be any solution. The droplet is too heavy and acoustic levitation is impossible. The case of interest in the present work is the one where the droplet weight is smaller than the maximum of F_L (vertical line 2 in figure 3), and there are two intersection points D and E on curves 1 and 2 in figure 3. It is known and easy to see that point D corresponds to a stable equilibrium, and point E to an unstable one. Thus, the value of L satisfying the overall force balance (4.1) should be taken in the range $\pi/4\Omega \lesssim L \lesssim \pi/2\Omega$ corresponding to point D in figure 3 ($\pi/4\Omega$ approximately corresponds to the maximum of the acoustic levitation force).

(iv) Given L, we find, as a result, the acoustic pressure distribution p_a over a supposed droplet shape, which also satisfies the overall force balance (4.13). Therefore, using this p_a we solve (4.7) with the conditions (4.8) and (4.9). In the present work, system (4.7) was integrated numerically by the Kutta–Merson method. Iterating C to satisfy (4.10) also, we find a new shape of the droplet. If it differs from the previous one more than allowed by a prescribed accuracy, the algorithm is applied once more, beginning from (ii).

When the iterations converge, we get a final droplet shape, as well as the acoustic pressure distribution on its surface p_a satisfying all the required conditions: (4.10), mass conservation condition, and the overall force balance (4.13).

Note that in (i) we use an initial guess of a droplet shape in the form of a sphere with the top at $z = 1$ (non-dimensional). Thus, in the first iteration $z_T = 1$ in (4.8c). As a result, the droplet top in the subsequent iterations is also located at $z = 1$. It is easy to see that in all the subsequent iterations we can always use the same value of $z_T = 1$, which does not affect the results.

Let the centre of the median cross-section of a droplet be below its top by a distance Δ along $(z+L)$-axis. Then the displacement of the centre from the pressure node, D, is given by

$$D = -\left[\frac{\pi}{2\Omega} - (L+1)\right] - \Delta \tag{4.14}$$

(for $z_T \equiv 1$). Note, that if Δ is a displacement of the centre of gravity of the droplet relative to its top (which is certainly distinct from the centre of the median cross-section), then (4.14) yields the displacement of the centre of gravity relative to the pressure node.

5. Results for steady-state droplet shapes: comparison with experiment and discussion

The levitator used in this study was supplied by Battelle-Frankfurt and is shown in figure 4. The acoustic wave is generated by a piezo crystal operated at a frequency of 56 kHz. The reflector is adjustable and was positioned to allow five nodes of a standing wave. The droplets were suspended in node three from the piezo transducer. The piezo transducer was 12 mm in diameter with a 2 mm central hole, used in a parallel study to produce a jet flow (Keller *et al.* 1995). The reflector was plane and 12 mm in diameter. No attempt was made to measure the divergence of the acoustic field and in all of our work a plane field was assumed. Further information on possible deviations from this assumption may be found in Lierke (1996).

To illuminate the droplet, a white light source was placed behind a white semi-opaque screen, positioned opposite a CCD camera. The camera was connected to the computer via a frame grabber interface. Software was available for processing of the digital images (Optimas). The experimental data obtained in the course of the present work are new.

It was not possible to monitor the droplet shape from the vertical direction to estimate deformations from the axisymmetric shape directly. Experimental data shown in figure 6 suggest, however, than in any case such a deformation should be very small compared to the drop size. It should be also mentioned that there are no self-sustained forces exciting non-axisymmetry and certainly we did not observe any corresponding oscillations on the screen.

We did not use a small microphone to measure the sound pressure. The reason for this is that most other studies which do use microphones involve considerably longer wavelengths, and thus larger dimensions. In the present levitator measurement with a microphone is not easy to do without disturbing the field.

With the goal of comparison with the experiment, all the corresponding calculations were made for droplets of n-hexadecane $C_{16}H_{34}$ possessing the following physical parameters: $\rho_l = 0.7734$ g cm^{-3}, $\alpha = 27.64$ g s^{-2}. The density and sound velocity of air were taken as $\rho_0 = 1.18 \times 10^{-3}$ g cm^{-3} and $c_0 = 3.4 \times 10^4$ cm s^{-1}, respectively.

For a given decibel level (dB_e), the amplitude of the pressure wave (2.5), A_{0e}, may be found from the equation (Morse 1948, p. 226)

$$dB_e = 20 \log_{10}(A_{0e}) + 74, \tag{5.1}$$

where A_{0e} is in dyne cm^{-2}, whereas from (2.6) the sound level in decibel, dB, corresponding to the amplitude at the sound source, A_0, is related to dB_e as

$$dB = dB_e + 20 \log_{10}[-\cos(\omega L_r / c_0)]. \tag{5.2}$$

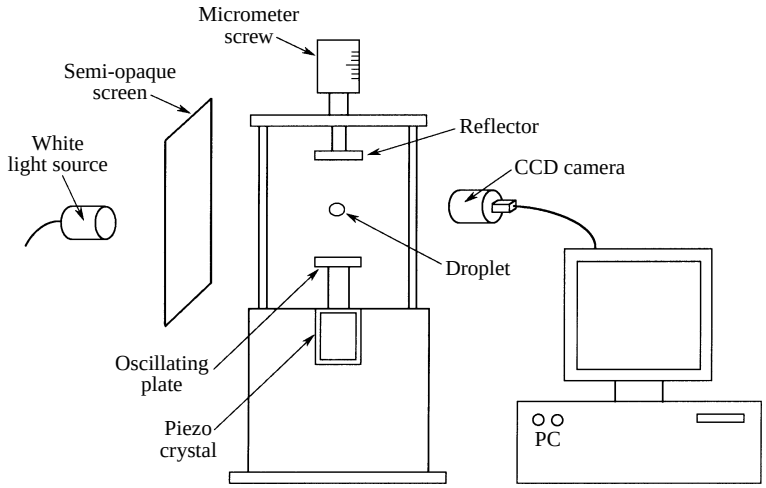

FIGURE 4. Schematic picture of the experimental set-up with the acoustic levitator and the imaging system for the determination of the droplet shape.

Under the conditions of the present experiment $20\log_{10}[-\cos(\omega L_r/c_0)] = -3.61$ for $L_r = 1.6$ cm.

Note that the definition of the sound pressure level (SPL) in decibel is based, as a rule, on the root-mean-square pressure amplitude p_{rms} (Morse 1948, p. 226). For a plane travelling wave $p_{rms} = A_{0e}/\sqrt{2}$, which yields a value of SPL lower than that of (5.1) and (5.2) by 3.01 decibel. For standing waves, we prefer to use the definition of (5.1).

Some insight into the link between the sound pressure level (SPL) and the driving voltage may be achieved by investigating a droplet levitated in the acoustic field without accounting for the droplet deformation from the spherical shape.

For a levitated sphere, the acoustic force has to compensate exactly the gravitational force. Equating King's (1934) force given by (3.3) with the droplet weight, we arrive at the following expression for A_{0e}:

$$A_{0e}^2 = \frac{4}{3}\frac{a_0\rho_l\rho_0 g c_0^2}{f_{King}(\Omega)\sin(2\Omega L)}, \tag{5.3}$$

where L is rendered dimensionless by a_0.

In the case when a spherical particle is levitated, a slow decrease in the driving voltage (at fixed reflector distance L_r) towards the minimum levitating voltage will lead to the positioning of the particle's centre at

$$L = \pi/4\Omega \tag{5.4}$$

(see figure 3). A further decrease of the driving voltage results in the dropout of the sphere because the acoustic force can no longer compensate the gravitational force. By inserting (5.4) into (5.3) the amplitude of the sound wave at the point of dropout can be calculated:

$$A_{0em}^2 = \frac{4}{3}\frac{a_0\rho_l\rho_0 g c_0^2}{f_{King}(\Omega)}. \tag{5.5}$$

This expression, together with (5.1) and (5.2) provides a means to experimentally determine the sound pressure level at the dropout condition for spheres.

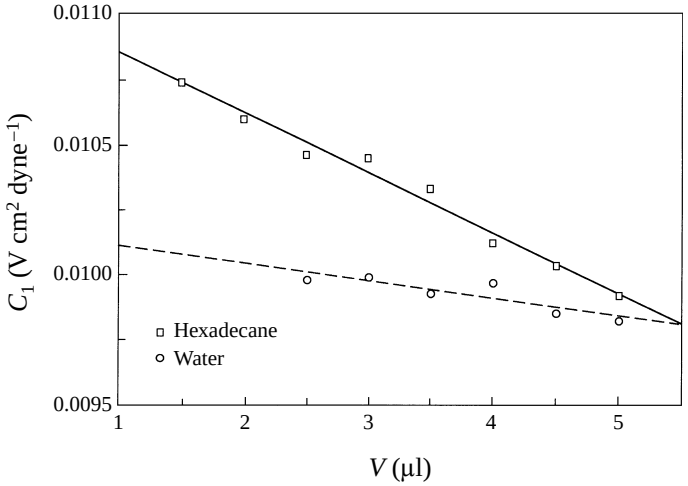

FIGURE 5. C_1 (the ratio of the driving voltage U_{0m} and the amplitude of the pressure wave A_{0em} at the point of dropout) for water and n-hexadecane droplets as a function of the droplet volume. The lines are linear interpolations.

The oscillation amplitude of the piezo transducer, which serves as the ultrasound source in the levitator, is assumed to be linearly proportional to the driving voltage applied to it. Neglecting nonlinear acoustic effects, which should be valid at the sound pressure levels used, one can also expect that the amplitude of the wave is linearly proportional to the oscillation amplitude of the transducer. Therefore the sound amplitude and driving voltage under the conditions of droplet levitation (A_{0e}, U_0) and dropout (A_{0em}, U_{0m}) are related as follows:

$$A_{0e} = A_{0em}\, U_0/U_{0m}. \tag{5.6}$$

It should be mentioned that the formulae (3.3), (3.4*b*) and (5.5) are valid only for spheres. The droplets however were slightly deformed, even at the moment of dropout. The effect of droplet deformation can be investigated by comparing the dropout sound pressure level for droplets of different surface tensions. For this purpose the dropout of water droplets, in addition to the n-hexadecane droplets, was investigated. Equation (5.6) predicts that the ratio of the sound wave amplitude A_{0e} to the driving voltage amplitude U_0 is constant:

$$\frac{U_0}{A_{0e}} = \frac{U_{0m}}{A_{0em}} = C_1. \tag{5.7}$$

Substituting (5.5) yields

$$U_{0m}\left(\frac{3}{4}\frac{f_{King}(\Omega)}{a_0\rho_l\rho_0 g c_0^2}\right)^{1/2} = C_1, \tag{5.8}$$

where C_1 on the right-hand side of (5.8) has to be constant for different fluids and droplet volumes, assuming no droplet deformation.

The left-hand side of (5.8) is plotted for different droplet volumes in figure 5 for both n-hexadecane and water. U_{0m}, the voltage at dropout, was found as the mean value of repeated readings for five identical droplets. The lines in figure 5 are linear interpolations of the experimental data. For water droplets, the variation of C_1 is marginal over the range of droplet volumes investigated, corresponding to a change of the acoustic field amplitude A_{0e} of 1.75%, or 0.15 $\mathrm{dB_e}$. The n-hexadecane droplets

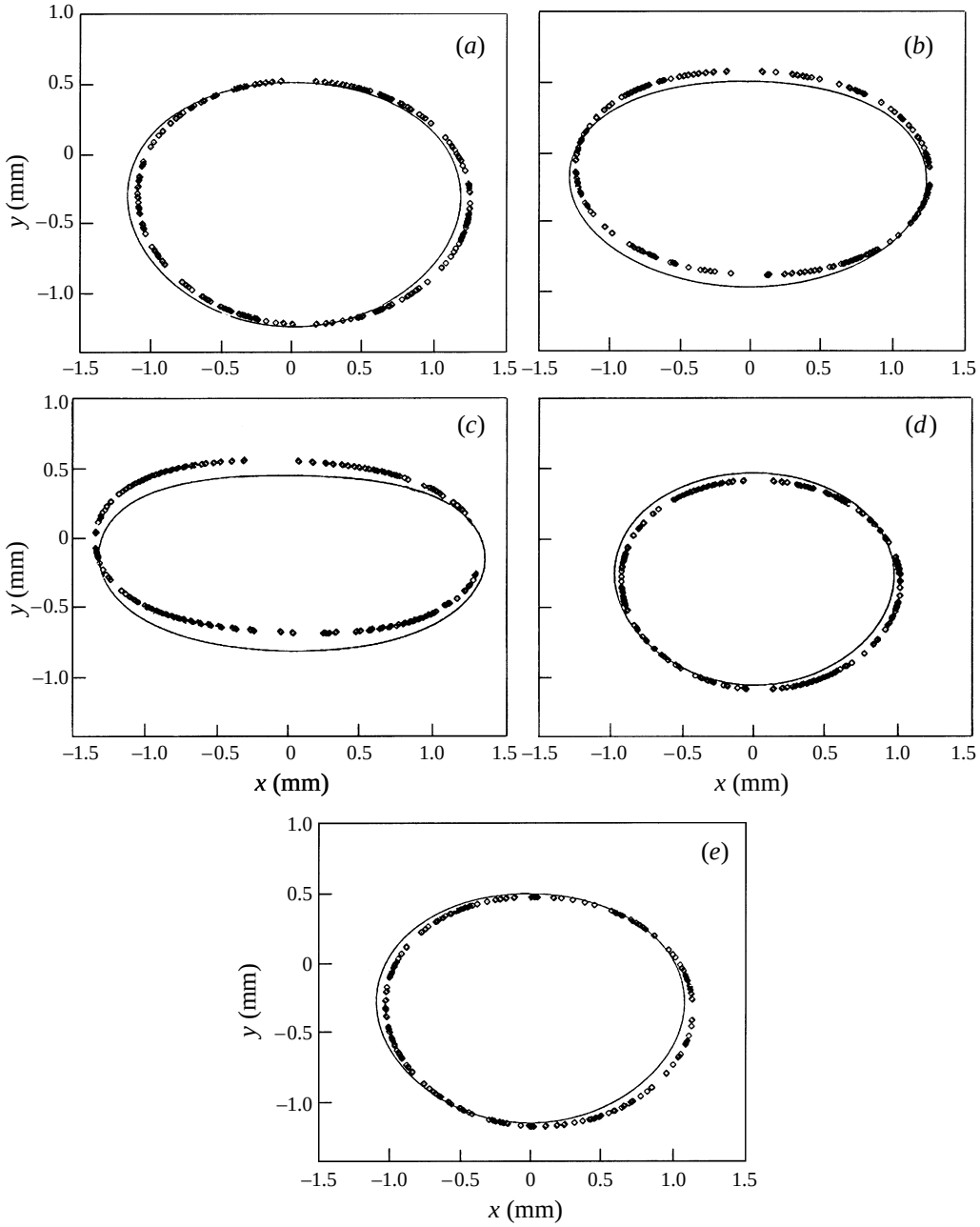

FIGURE 6. Droplet shapes: theory vs. experiment. Theoretical results are shown by curves, experimental data by symbols with details listed in table 2. (*a*) Experiment No. 1: $Bo = 0.3086$, $We_a = 5235.15$, $\Omega = 1.0978$, $A_{0e}/\rho_0 c_0^2 = 0.0150$. (*b*) Experiment No. 2: $Bo = 0.3086$, $We_a = 5235.15$, $\Omega = 1.0978$, $A_{0e}/\rho_0 c_0^2 = 0.0175$. (*c*) Experiment No. 3: $Bo = 0.3086$, $We_a = 5235.15$, $\Omega = 1.0978$, $A_{0e}/\rho_0 c_0^2 = 0.0189$. (*d*) Experiment No. 4: $Bo = 0.2195$, $We_a = 4415.49$, $\Omega = 0.9259$, $A_{0e}/\rho_0 c_0^2 = 0.0150$. (*e*) Experiment No. 5: $Bo = 0.2659$, $We_a = 4859.88$, $\Omega = 1.0191$, $A_{0e}/\rho_0 c_0^2 = 0.0150$. The origin of the coordinates is at the pressure node ($y = 0$ in the present figure corresponds to $z + L = \pi/2\Omega$ in figure 3).

Experiment no.	Voltage (V)	Drop volume (μl)	a_0 (μm)	Displacement, theory/exp. (μm/μm)	Aspect ratio, theory/exp.
1	156	5	1061	−335.33/−340	1.3530/1.3530
2	197	5	1061	−194.77/−141	1.7120/1.7131
3	238	5	1061	−138.86/−52	2.1507/2.1504
4	156	3	895	−276.13/−328	1.2837/1.3071
5	156	4	985	−300.26/−337	1.3277/1.3530

TABLE 2. Displacements of the median cross-section and aspect ratios: theory vs. experiment. Uncertainty in drop volume ±1%, in cross-section and displacement ±40 μm and in aspect ratios ±3%.

exhibit a higher variation of C_1 (7.5%, or 0.6 dB_e), which can also be expected, due to the larger deformations resulting from the lower surface tension.

There exist some experimental uncertainties in the measurements presented in figure 5. The droplets were injected into the levitator using a precision syringe, with an estimated uncertainty in the droplet volume of ±1%. Effects of evaporation are considered to be negligible for the period of time required to perform the dropout experiment. The value of c_0, however, undergoes small variations with temperature and humidity, estimated to be of the order of ±1% for typical room value fluctuations (±5 °C, ±20% RH). No conclusive information is available about the variation of surface tension of the distilled water and n-hexadecane used, especially with respect to impurities, since only spot check measurements were performed. The surface tension will enter the measurements of figure 5 through the degree of deformation of the droplet.

Some variations of C_1 are observed from day to day; however, if experiments with water and n-hexadecane are performed immediately after one another, the value C_1 for water will always be larger, typically 1–7% for a 5 μl droplet. The higher surface tension of water and hence the weaker deformation (lower aspect ratio) at the same SPL, together with figure 5, is a first indication that King's formula overestimates the SPL if it is applied to deformed droplets.

Next the aspect ratio and the displacement of droplets are determined by evaluating digital pictures taken with the CCD camera and using the image processing software. The link between the aspect ratio and A_{0e} is investigated for several reflector distances. Daidzic (1995) has already investigated the dependence of the aspect ratio on what he called the acoustic power for one reflector distance. In fact this power is an arbitrary electric power which is more or less proportional to the electric power applied to the piezo crystal. Daidzic did not determine A_{0e} explicitly, nor did he find its influence on the aspect ratio.

The experimental results obtained by the CCD camera and software are shown in figure 6 (with symbols) and tables 2 and 3. The measurement of absolute displacement using the CCD camera requires a calibration, which leads to uncertainties of ±40 μm. These uncertainties become significant, especially for smaller displacements. However, the measurement of the aspect ratio does not rely on a calibration and is limited in its accuracy only by the image resolution. An overall accuracy of the measured aspect ratio of ±3% has been estimated. It is emphasized that droplet shape and displacement are both a strong function of the acoustic pressure as is seen from table 2 (also curve 1 in figure 9).

By means of the numerical algorithm outlined in §2 and §4, we first made

Voltage (V)	Aspect ratio
156	1.3530
197	1.7131
238	2.1504

TABLE 3. Aspect ratio vs. driving voltage for a 5 μl droplet obtained in the experiment. Uncertainty of measured aspect ratio ±3%.

Voltage (V)	dB_e	dB resulting from the calibration	dB found experimentally by another method for the same set-up (Keller *et al.* 1995)
156	160.247	156.64	156.78
197	161.573	157.96	157.98
238	162.241	158.63	158.27

TABLE 4. Voltage–decibel link; $L_r = 1.6$ cm.

calculations for a n-hexadecane 5 μl volume droplet for different sound levels. In the steady state, the droplet cross-section was squeezed by the acoustic field and became oblate. These calculations resulted in a theoretical dependence of the aspect ratio of the squeezed cross-section on decibel level dB_e (SPL). This dependence is shown by curve 1 in figure 9. It was used for calibration of the levitator together with data for the aspect ratio of a 5 μl droplet found in the experiment for different values of driving voltage (shown in table 3). Using the data shown by curve 1 in figure 9, via linear interpolation, we found dB_e-levels corresponding to the experimental aspect ratios of table 3. Thus, a link was established between the driving voltage and dB_e, as well as the dB level (see (5.2)), presented in table 4. The experimental data of table 4 were found independently by Keller *et al.* (1995) using another method and will be published in detail elsewhere. Note briefly that Keller *et al.* (1995) calibrated the SPL of the levitator by a direct measurement of the displacement velocity amplitude in the sound wave, as well as via the mean velocity variation along the levitator axis when a laminar submerged gas jet was issued axially. The accuracy of the method of Keller *et al.* (1995) was estimated as ±0.43 dB. Note also that Keller *et al.* (1995) defined SPL as in (5.1) and (5.2). It is seen that the results of the present calibration method agree with those of Keller *et al.* (1995) (cf. the third and the fourth columns in table 4). The accuracy of the present method is estimated as ±0.09 dB.

The good agreement between the theory and experiment shown in table 4 for $L_r = 1.6$ cm deserves some more comments. In the experiment of Keller *et al.* (1995) the accuracy of measurements of reflector distance L_r was not high enough to distinguish the second decimal digit. The value of dB from (5.2) is, however, highly sensitive to the value of L_r. For example, for $L_r = 1.605$ cm and $L_r = 1.61$ cm calculated values of dB will differ from those of table 4 by 0.53 dB and 1.136 dB, respectively.

The voltage–decibel link found for a 5 μl droplet will be used henceforth without any change in numerical calculations of shapes and displacements of 3, 4 and 5 μl n-hexadecane droplets.

We compared droplet shapes calculated numerically and found experimentally. We also compared the corresponding displacements of the centre of the droplet median

cross-section. The results are shown in figure 6 and table 2. The origin of the coordinates in figure 6 is located at the pressure node. Thus, $y = 0$ in figure 6 corresponds to $z + L = \pi/2\Omega$ in figure 3.

A similar comparison was done by Tian *et al.* (1993) for a water drop of aspect ratio less than about 1.55. (They also made calculations for several other fluids.) It showed that their approximate theory is valid in this range of aspect ratios. Comparison of the aspect ratios with experimental data for relatively small values of Ω (without considering the whole droplet shape and displacement) showed that for some other fluids the agreement of the theoretical results of Tian *et al.* (1993) might be good at aspect ratios close to 2. Regarding a comparison for droplets of silicon oil in the latter work, Shi & Apfel (1996) commented that 'the computations ... grow too fast as the sound pressure increases'.

The main difference between the method of Tian *et al.* (1993) and the present one is in the numerical calculation of the scattered acoustic field, as well as in the calculation of the squeezed droplet shape. The scattered field in Tian *et al.* (1993) was represented by a series in spherical functions, which was truncated at the third term. They also fitted the droplet shape by a nonlinear least-squares fitting.

The present method directly calculates the radiation pressure at the nodal points on the droplet surface, as well as numerically solving the differential equations governing droplet shape. The accuracy of the present method smoothly increases with the number of nodal points. Note that the results of figure 6 were obtained with $N = 51$ nodal points per half-loop of the generatrix used in the calculation of the acoustic radiation pressure by the BEM. Preliminary calculations with 31 and 101 nodal points showed that $N = 51$ is a reasonable compromise between accuracy and time consumption.

The voltage–decibel link, once established (refer to table 4), was used without any fitting to calculate droplet shapes and displacements from the pressure node. The theoretical droplet shapes are plotted in figure 6 by curves together with the experimental data taken by the CCD camera with Optimas software and shown by symbols.

The present experimental data for n-hexadecane drops include aspect ratios up to 2.15; the data are compared with the theory valid for any aspect ratio which may be achieved in a steady state.

The results shown in figure 6 and table 2 allow us to conclude that the theory reproduces rather accurately the droplet shapes, including the aspect ratios. The agreement for the displacement is somewhat poorer, as especially seen in figure 6(*b*, *c*) and from the corresponding data in table 2. It should be mentioned, however, that the experimental data plotted by symbols in figure 6 show some lateral asymmetry relative to the vertical axis $x = 0$ (the theoretical results shown by curves in this figure are totally symmetric, and may be used to detect deviations from the symmetry in the experimental data). The scale of these asymmetries is of the order of the disagreement between the theoretical and experimental data for the displacement present in table 2. Therefore, most of the discrepancies between the theoretical and experimental data for the centre displacement may be attributed to the inaccuracy in measurement of droplet location. The overall droplet shape is not sensitive to these discrepancies and continues to be very close in the theory and experiment, as follows from figure 6. It is emphasized that droplet shape and displacement are both a strong function of the acoustic pressure as is seen from table 2 (also see curve 1 in figure 9).

Small lateral asymmetries of the experimental data in figure 6 relative to $x = 0$ may be partly attributed to a radial distribution of the acoustic field tending to stabilize droplets at the levitator axis, which does not preclude, however, small oscillations of

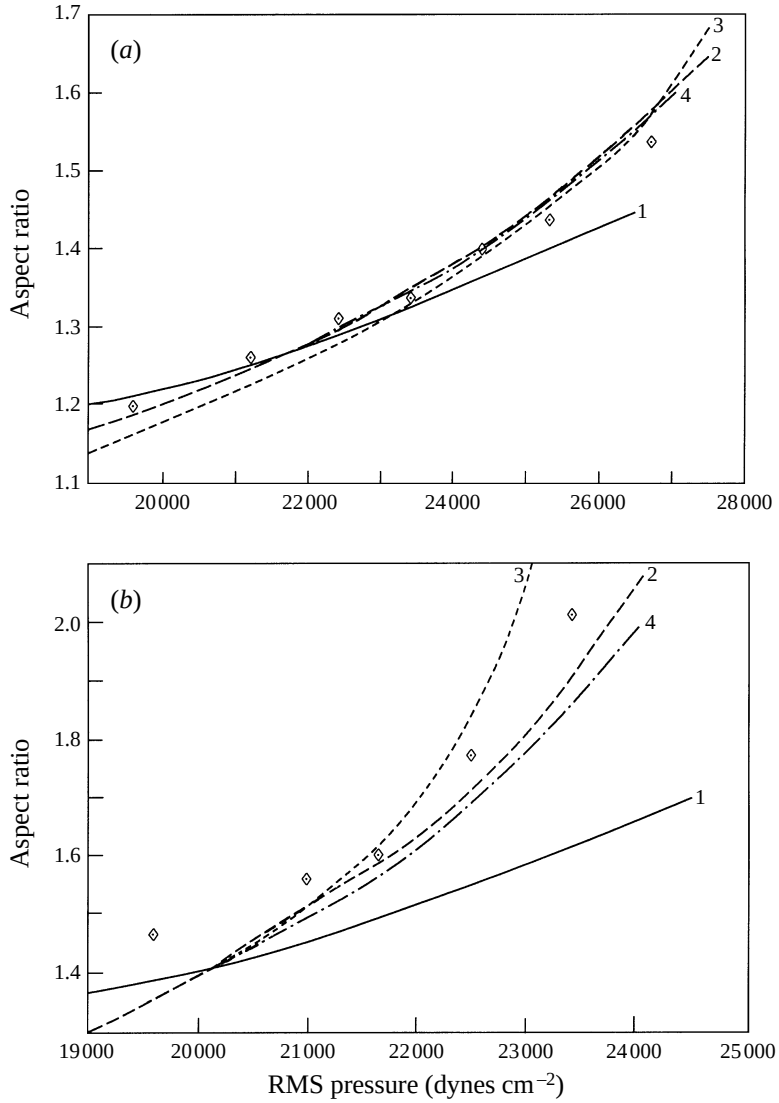

FIGURE 7. Comparison of the present theory with the experimental data of Trinh & Hsu (1986) and some other theoretical methods. Symbols: the data of Trinh & Hsu (1986) for silicone oil droplets ($\rho = 0.95$ g cm^{-3}, $\alpha = 20$ g s^{-2}). (*a*) $a_0 = 0.045$ cm, $\Omega = 0.16$; (*b*) $a_0 = 0.07$ cm, $\Omega = 0.25$. The error bars of the experimental data for the aspect ratio are not less than about 0.1. Curves show the predictions of theory: curve 1, Marston (1980); 2, Shi & Apfel (1996); 3, Tian *et al.* (1993); 4, the present work.

the droplet position due to its inertia. Some instantaneous random air currents or table vibrations also could not be eliminated totally. As a result, small oscillations of droplet position might be caught on a snapshot.

The fact that measured and predicted droplet contours in figure 6 may be superimposed perfectly by small shifts in horizontal and vertical directions (without any shape modifications) also supports the assumption that small, almost instantaneous, variations of droplet position could be attributed to the above-mentioned factors. If any sustained non-axisymmetry were involved that would not be the case.

We also compared our theoretical method with the experimental data of Trinh &

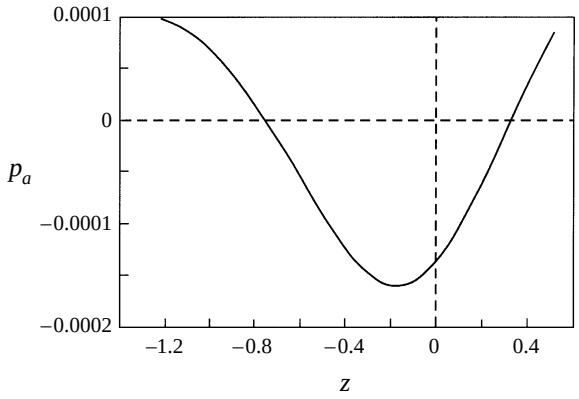

FIGURE 8. Acoustic radiation pressure distribution calculated for experiment No. 1 from table 2. The highest z corresponds to the top of the droplet, the lowest to the bottom.

Hsu (1986), approximate theories of Marston (1980) and Tian *et al.* (1993), as well as with recent numerical results of Shi & Apfel (1996). The results for two droplets of silicone oil are presented in figure 7. It is seen that the methods of the present work and of Shi & Apfel (1996) yield rather close results in the whole range of variation of the acoustic pressure (measured by a probe microphone) and fit experimental data sufficiently accurately. The analytical results significantly underestimate the experimental data, whereas the approximate computations overestimate them.

Anilkumar *et al.* (1993*b*) in their figure 9 presented experimental data for the critical values of the acoustic Bond number B_a and critical non-dimensional equatorial radius b/a_0 corresponding to disappearance of a steady simple oblate shape of water droplets. The Bond number Bo given by (4.5*b*) calculated for their experimental data varies from 0.14 to 0.46 which is close enough to the range of Bo in the present work (0.22–0.31, as is seen in the caption to figure 6). Therefore it is worth comparing their experimental results with the theoretical predictions for one of our cases which is rather close to the disappearance of the steady simple oblate shape (given by figure 6*c*). In our notation $B_a = (A_{0e}/\rho_0 c_0^2)^2 We_a$. Therefore $B_a = 1.87$ and $b/a_0 = 1.666$ for our figure 6(*c*) corresponding to $\Omega = 1.0978$ (the value of b/a_0 is found from the aspect ratio b/a as $(b/a)^{2/3}$ like for a spheroid). The data of figure 9 of Anilkumar *et al.* (1993*b*) extend only up to $\Omega = 0.74$. A reasonable extrapolation of their results to $\Omega = 1.0978$ shows good agreement with our values of $B_a = 1.87$ and $b/a_0 = 1.666$.

From table 2 it is seen that the displacement D is approximately 10–30 % of the unperturbed droplet radius a_0. The computations of the present work show that in the experiments of Trinh & Hsu (1986) the displacements D sometimes constitute more than 150 % of the unperturbed droplet radius. Therefore, in the given case the displacement definitely cannot be ignored, as was assumed in Lee *et al.* (1994).

A distribution of the acoustic radiation pressure over a half-loop of the generatrix is plotted in figure 8 against z-values corresponding to the points along the generatrix. It is seen that the droplet top (near $z = 0.5$) and bottom (near $z = -1.2$) are compressed ($p_a > 0$), whereas the equatorial part $-0.7 \lesssim z \lesssim 0.3$ is stressed ($p_a < 0$) by the acoustic radiation pressure. Asymmetry relative to the equator evidently arises due to droplet displacement relative to the pressure node.

Note that the normalized lengths of the half-loop of the generatrix of the droplet surfaces in figure 6 obtained numerically are less than that of the unperturbed droplets. This may be explained by the fact that the shapes of the droplets presented in figure

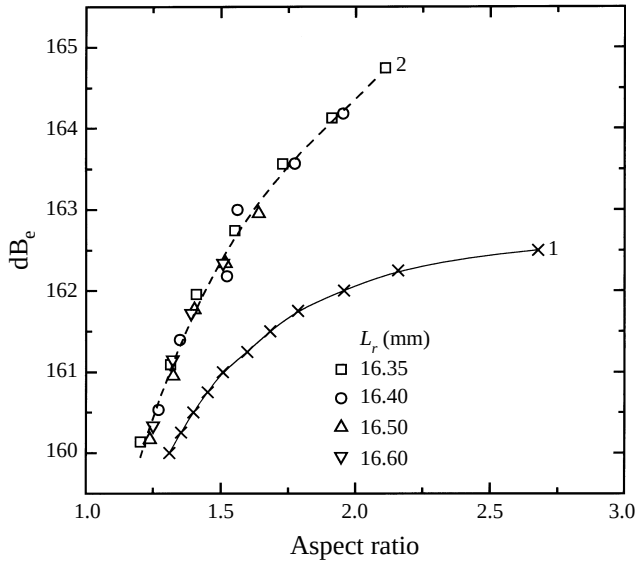

FIGURE 9. SPL vs. the aspect ratio for 5 μl n-hexadecane droplets. The results for several reflector distances L_r are determined via equation (5.6) and interpolated with a polynomial fit (curve 2). There are four measurement series corresponding to four values of L_r. The point with the highest dB_e value for each measurement series refers to the same value of driving voltage amplitude U_0. There are four distinct points of this type corresponding to four values of L_r. The data are compared with the calibration data obtained by the BEM (curve 1).

6 are close to spheroids. The volume of a spheroid with an ellipse in the median cross-section is equal to

$$\tfrac{4}{3}\pi ab^2 = \tfrac{4}{3}\pi a_0^3, \tag{5.9}$$

where a and b are the semi-axes of the ellipse, and a_0 is the unperturbed droplet radius (a corresponds to the y-axis and b to the x-axis in figure 6). The length of the half-loop of the generatrix of elliptic shape is given accurately enough by the left-hand side of

$$\tfrac{1}{2}\pi[1.5(a+b)-(ab)^{1/2}] < \pi a_0, \tag{5.10}$$

which should be compared with that of a circle (for the unperturbed droplet) πa_0. Under the condition (5.9), the inequality (5.10) reduces to

$$1.5(b^{-2}+b)-b^{-1/2} < 2, \tag{5.11}$$

where b is rendered dimensionless by a_0. The inequality (5.11) is satisfied for $1 < b \lesssim 1.375$. Therefore, it is satisfied for all ellipses with aspect ratios less than $b/a = b^3 = 1.375^3 = 2.6$. The latter is the case for all the results presented in figure 6, which explains why the corresponding lengths of the half-loop of the generatrix are less than that of the unperturbed spherical droplet.

At higher levels of the driving voltage $U_0 > U_{0m}$, where stable levitation of droplets is achieved, the droplet is squeezed by the acoustic field, as seen in figure 6. It is worth estimating the range of applicability of the sphere-based formulae (3.3), (3.4*b*), as well as (5.3) for the levitation force and SPL under the conditions of growing droplet deformation, i.e. increasing aspect ratio. To do this, using (5.1), (5.2) and (5.3) we calculated the SPL in decibel dB_e corresponding to several cases of droplet levitation in the experiments, and plotted the measured SPL against the aspect ratio in figure 9 for 5 μl n-hexadecane droplets. Results for various reflector positions, and hence various values of L_r, are fitted with a dashed interpolation curve. It is clear that the

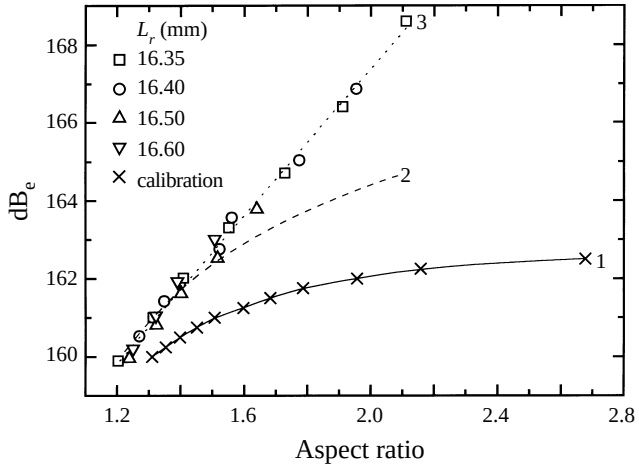

FIGURE 10. SPL vs. the aspect ratio for 5 μl n-hexadecane droplets. The results for several reflector distances L_r are determined by measuring the displacement of the droplet cross-section centre from the pressure node, calculating the displacement L from the pressure antinode and inserting L into King's formula (5.3). Curve 3 is a polynomial interpolation of the results. The results are compared with the calibration curve 1 and curve 2, which is the polynomial interpolation of the results of using equation (5.6). Curves 1 and 2 are also shown in figure 9.

aspect ratio is not a function of the reflector position and the driving voltage but rather of A_{0e}, which is a function of each of these two quantities from equation (2.6).

Also plotted in figure 9 is the theoretical calibration curve 1, which is in agreement with the droplet images. The discrepancy observed between theory and experiment in figure 9 can be attributed to the non-validity of King's result at higher SPL due to droplet deformation from the spherical state, consistent with the results shown in figure 5. Possibly also the 'mechanical' assumption of equation (5.6) may lose validity at higher amplitudes. This assumption was therefore tested by measuring directly the motion of the piezo-transducer using an LDA focused onto the surface of the transducer. The results showed linearity between the applied control voltage and the transducer displacement over the entire working range of the device, thus confirming equation (5.6).

Nevertheless, an alternative method of computing SPL, which does not rely on equation (5.6), is also available. In this case the SPL is derived from the droplet displacement, according to (5.1), (5.2) and (5.3). The result of this computation is shown in figure 10, together with the two previous curves of figure 9. Curve 3 in figure 10 is still far from curve 1 at aspect ratios above 1.2. This discrepancy now may be attributed solely to droplet deformation, which is not accounted for by King's model. The fact that King's model fails for deformed droplets may be expected. However, the range of approximate validity of King's formula for slightly deformed droplets deserves investigation, since it shows the range of validity of sound pressure calibration methods using small droplets. From figure 10 we can conclude that the droplet deformation cannot be neglected and King's relationship for the levitation force is inapplicable for aspect ratios much beyond 1.2.

With regard to the previous measurements based on the droplet displacement from the pressure node, some consideration of the measurement accuracy is necessary. The location of the pressure node is determined by finding the position of a levitated polystyrene sphere. Due to its finite mass however, there exists a small bias error, which has not been corrected for, i.e. the sphere will lie marginally below the pressure node.

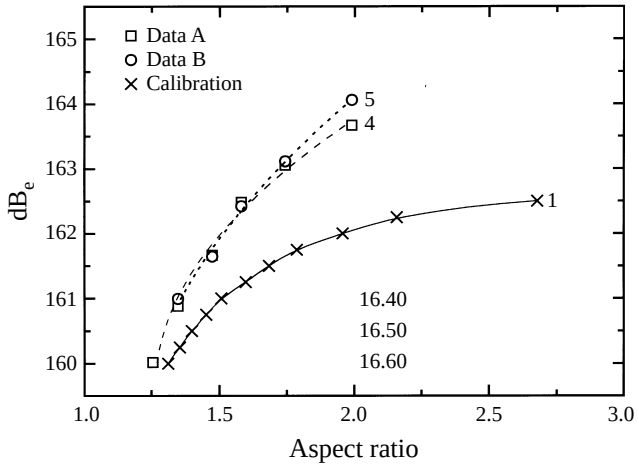

FIGURE 11. SPL vs. the aspect ratio for 5 μl n-hexadecane droplets for a reflector distance L_r of about 1.63 cm. In contrast to figures 9 and 10 the SPL of data A and B is determined using water droplets for calibration of SPL. All the results shown correspond to n-hexadecane. Data A are determined using equation (5.6), whereas data B are calculated by measuring the displacement of the droplet cross-section centre from the pressure node, calculating the displacement L from the pressure antinode and inserting L into King's formula (5.3). The results are compared with the calibration curve 1 obtained by the BEM model.

Additionally, there is some uncertainty in the displacement measurement due to lateral asymmetry, as discussed in reference to figure 6 and due to the calibration of the image resolution. Although the magnitude of the error remains at approximately 3%, the sinusoidal relation between displacement and the sound pressure amplitude (5.3) results in larger absolute errors in A_{0e}. The overall accuracy of the SPL measurement is about ± 0.09 dB if a very small and light spherical particle is used.

A further way to investigate the influence of the aspect ratio on the validity of King's result is to determine the SPL for water droplets. Water droplets show at the same SPL a smaller aspect ratio than n-hexadecane droplets due to their higher surface tension. The deviation of King's results from the calibration curve 1 in figure 9 should be smaller than the deviation of the results using n-hexadecane to determine the SPL. Figure 11 shows the SPL as a function of the aspect ratio of n-hexadecane droplets for a reflector distance L_r of about 1.63 cm. The SPL was determined with water droplets by finding the voltage of dropout and assuming a linear dependence between the sound pressure amplitude and the driving voltage via (5.6) (data A and curve 4 in figure 11) and by measuring directly the displacement from the pressure node (data B and curve 5 in figure 11). Water droplets were used for calibration of SPL only and all the results of figure 11 correspond to n-hexadecane. The deviations of curves 4 and 5 from curve 1 are smaller than the deviations of curves 2 and 3 shown in figures 9 and 10. But still the effect of the droplet deformation can be clearly seen. Due to the larger displacement of water droplets from the pressure node, and hence the higher accuracy of the displacement measurement, there is a good agreement between the results using equation (5.6) and the results derived from the displacement measurements, even up to higher levels of the SPL.

Figure 12 shows the SPL of n-hexadecane droplets of different volumes as a function of the aspect ratio. The SPL is again determined using water droplets for its calibration. Figure 12 unambiguously shows that the smaller the droplet size, the less the discrepancy between the values of the SPL calculated with two different methods. This

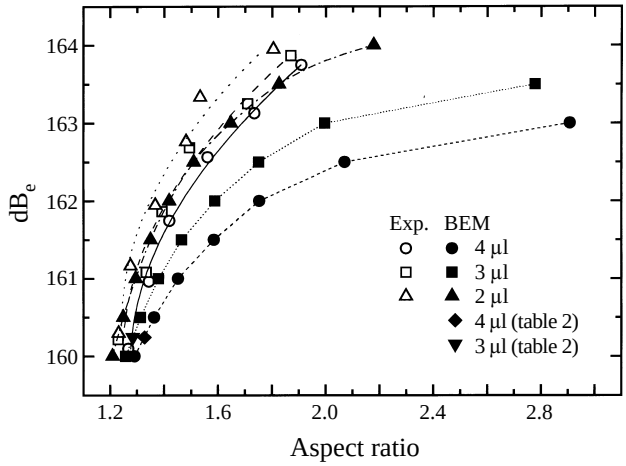

FIGURE 12. SPL vs. the aspect ratio for n-hexadecane droplets of different volumes for a reflector distance L_r of about 1.63 cm. The SPL was determined using water droplets (only for calibration) and equation (5.6). The results are compared with the predictions of the BEM accounting for the droplet deformation. The experimental data for 2, 3 and 4 μl droplets are shown by the open symbols and interpolated by curves. The BEM results are shown by the corresponding solid symbols (also interpolated by curves). Two points obtained by the BEM for 3 and 4 μl droplets and corresponding to the data of table 2 are also shown.

results from the fact that smaller droplets are less deformed by the acoustic field. Therefore, the sound pressure calibration method based on equation (5.6) becomes more accurate.

6. Conclusions

A novel method of calculation of shapes of acoustically levitated droplets was developed. It is based on a numerical solution of the boundary integral equation describing the distribution of the acoustic radiation pressure over a droplet surface. Combined with the overall and pointwise (over the droplet surface) force balance, it allowed us to find both droplet shape and displacement from the pressure node.

An experimental set-up was constructed to measure droplet shapes and displacements from the pressure node.

Comparison of the theoretical predictions for the droplet aspect ratio with the corresponding experimental data obtained in the present paper allowed us to establish a link between the sound pressure level (SPL) and the parameters of the levitator (its driving voltage and reflector distance). Therefore the approach developed in the present paper may serve as a new method of levitator calibration, valid for large drops.

Theoretical results for droplet shapes are in good agreement with the corresponding experimental data obtained in the present paper and found in the literature. The agreement between the theoretical and experimental data for the displacements of droplet centres from the pressure node is somewhat poorer, which was attributed to a less accurate measurement of droplet location.

The shapes of all the droplets in the present experiment were close to spheroidal. Their displacements from the pressure node were approximately 10–30 % of the unperturbed droplet radius a_0. For the experimental data of Trinh & Hsu (1986) displacements more than 150 % were found. These definitely cannot be ignored as assumed in Lee *et al.* (1994).

The approximate formula for the acoustic levitation force acting on a rigid sphere proposed in Leung *et al*. (1981), Lierke *et al*. (1983) and Lierke (1996) was found to be inaccurate outside its formal validity range (as it is frequently used). For sound wavelengths comparable with the sphere radius (e.g. in the present case it was $\Omega = ka_0 = \omega a_0/c_0 \approx 1$) its predictions differ by 16–19.6% from the exact ones obtained by King's (1934) formula or numerically.

King's (1934) formula for the acoustic levitation force acting on a sphere may be approximately applied to levitated droplets (which are non-spherical due to the squeezing action of the acoustic field) only up to the aspect ratios of about 1.2, which shows the range of validity of probe calibration methods.

A. L. Y. is indebted to the Lehrstuhl für Strömungsmechanik in the Universität Erlangen-Nürnberg in Erlangen for partial financial assistance and for their hospitality in 1995 and 1996. This research was partially supported by the Technion V. P. R. Elson/Shapiro Families Research Fund. The Deutsche Forschungsgemeinschaft supplied partial funding for this work through grant Br 1046/3.

Appendix

The following functions are involved in calculations of the kernels in equations (2.12):

$$Y(M,A) = \frac{\pi}{4}\int_{-1}^{1} \frac{\cos\{(\omega A^{1/2}/c_0)\,[1 - M\sin^2[(\pi/4)\,(\gamma+1)]]^{1/2}\}}{\{1 - M\sin^2[(\pi/4)\,(\gamma+1)]\}^{1/2}}\,\mathrm{d}\gamma, \qquad (A\,1a)$$

$$F(M,A) = \frac{\pi}{4}\int_{-1}^{1} \frac{\sin\{(\omega A^{1/2}/c_0)\,[1 - M\sin^2[(\pi/4)\,(\gamma+1)]]^{1/2}\}}{\{1 - M\sin^2[(\pi/4)\,(\gamma+1)]\}^{1/2}}\,\mathrm{d}\gamma, \qquad (A\,1b)$$

where the radial and axial coordinates of points Q and P on the droplet (or particle) generatrix (r, z) and (R, Z), respectively, are used to obtain

$$A = (R+r)^2 + (Z-z)^2, \quad M = \frac{4Rr}{(R+r)^2 + (Z-z)^2}. \qquad (A\,2a, b)$$

Differentiating (A 1), we find $Y_M = \partial Y/\partial M$, $Y_A = \partial Y/\partial A$, $F_M = \partial F/\partial M$, and $F_A = \partial F/\partial A$, and then

$$W_r = \frac{Y_M}{A^{1/2}}\frac{\partial M}{\partial r} + \frac{Y_A}{A^{1/2}}\frac{\partial A}{\partial r} - \frac{1}{2}\frac{Y}{A^{3/2}}\frac{\partial A}{\partial r}, \quad W_i = \frac{F_M}{A^{1/2}}\frac{\partial M}{\partial r} + \frac{F_A}{A^{1/2}}\frac{\partial A}{\partial r} - \frac{1}{2}\frac{F}{A^{3/2}}\frac{\partial A}{\partial r}, \qquad (A\,3a, b)$$

$$U_r = \frac{Y_M}{A^{1/2}}\frac{\partial M}{\partial z} + \frac{Y_A}{A^{1/2}}\frac{\partial A}{\partial z} - \frac{1}{2}\frac{Y}{A^{3/2}}\frac{\partial A}{\partial z}, \quad U_i = \frac{F_M}{A^{1/2}}\frac{\partial M}{\partial z} + \frac{F_A}{A^{1/2}}\frac{\partial A}{\partial z} - \frac{1}{2}\frac{F}{A^{3/2}}\frac{\partial A}{\partial z}, \qquad (A\,3c, d)$$

where the derivatives of M and A are calculated using (A 2).

With r, z, R, Z, L, and s rendered dimensionless by the unperturbed droplet radius a_0, the kernels in (2.12) take the form

$$G_1(P,Q) = \frac{2r}{\pi}\left(-W_r\frac{\partial z}{\partial s} + U_r\frac{\partial r}{\partial s}\right), \quad H_1(P,Q) = -\frac{2r}{\pi}\left(-W_i\frac{\partial z}{\partial s} + U_i\frac{\partial r}{\partial s}\right), \qquad (A\,4a, b)$$

$$G_2(P,Q) = -H_1(P,Q), \quad H_2(P,Q) = G_1(P,Q), \qquad (A\,4c, d)$$

$$M_1 = \frac{2}{\pi}\Omega\frac{\partial r}{\partial s}\sin[\Omega(z+L)]\frac{rY}{A^{1/2}}, \quad M_2 = \frac{2}{\pi}\Omega\frac{\partial r}{\partial s}\sin[\Omega(z+L)]\frac{rF}{A^{1/2}}, \qquad (A\,4e, f)$$

$$\Omega = \omega a_0/c_0. \qquad (A\,4g)$$

It may be shown that when point Q tends to point P, and point P does not belong to the droplet (or particle) axis ($R \neq 0$), the kernels G_1, H_2, and M_1 are logarithmically singular, whereas H_1, G_2 and M_2 are regular. When point Q tends to point P located at the droplet axis ($R = 0$), all the kernels are regular.

REFERENCES

Anilkumar, A. V., Lee, C. P. & Lin, K. C. 1993*a* Bifurcation of rotating liquid drops: results from USML-1 experiments in Space. *Center Report*, *Center for Microgravity Research and Applications*, *Vanderbilt University*, *Nashville*, *Tennesee*, p. 31.

Anilkumar, A. V., Lee, C. P. & Wang, T. G. 1993*b* Stability of an acoustically levitated and flattened drop: An experimental study. *Phys. Fluids* A **5**, 2763.

Apfel, R. E. 1971 A novel technique for measuring the strength of liquids. *J. Acoust. Soc. Am.* **49**, 145.

Basaran, O. A. 1992 Nonlinear oscillations of viscous liquid drops. *J. Fluid Mech.* **241**, 169.

Becker, A. A. 1992 *The Boundary Element Method in Engineering. A Complete Course*. McGraw-Hill.

Becker, E., Hiller, W. J. & Kowalewski, T. A. 1991 Experimental and theoretical investigation of large-amplitude oscillations of liquid droplets. *J. Fluid Mech.* **231**, 189.

Becker, E., Hiller, W. J. & Kowalewski, T. A. 1994 Nonlinear dynamics of viscous droplets. *J. Fluid Mech.* **258**, 191.

Daidzic, N. 1995 Nonlinear droplet oscillations and evaporation in an ultrasonic levitator. PhD thesis, Lehrstuhl fuer Stroemungsmechanik, Friedrich-Alexander-Universitaet Erlangen.

Goldshtik, M. A., Khanin, V. M. & Ligai, V. G. 1986 A liquid drop on an air cushion as an analogue of Leidenfrost boiling. *J. Fluid Mech.* **166**, 1.

Jaswon, M. A. & Symm, G. T. 1977 *Integral Equation Methods in Potential Theory and Elastostatics*. Academic.

Keller, J., Pfaffenlehner, M., Ryssel, E., Tropea, C., Yarin, A. L. & Daidzic, N. 1995 Aerodynamic-acoustic levitator for high Reynolds number applications. *Ultrasonics World Congress 1995 Proceedings*, *Berlin*, pp. 827–830.

King, L. V. 1934 On the acoustic radiation pressure on spheres. *Proc. R. Soc. Lond.* A **147**, 212.

Lamb, H. 1959 *Hydrodynamics*. Cambridge University Press.

Landau, L. D. & Lifshitz, E. M. 1959 *Fluid Mechanics*. Pergamon.

Lee, C. P., Anilkumar, A. V. & Wang, T. G. 1991 Static shape and instability of an acoustically levitated liquid drop. *Phys. Fluids* A **3**, 2497.

Lee, C. P., Anilkumar, A. V. & Wang, T. G. 1994 Static shape of an acoustically levitated drop with wave-drop interaction. *Phys. Fluids* **6**, 3554.

Leung, E., Jacobi, N. & Wang, T. 1981 Acoustic radiation force on a rigid sphere in a resonance chamber. *J. Acoust. Soc. Am.* **70**, 1962.

Lierke, E. G. 1996 Akustische Positionierung – Ein umfassender Ueberblick, ueber Grundlagen und Anwendungen. *Acta Acustica* **82**, 220.

Lierke, E. G., Grossbach, R., Floegel, K. & Clancy, P. 1983 Acoustic positioning for space processing of materials science samples in mirror furnaces. *IEEE Ultrasonics Symposion*, *Atlanta*, p. 1129.

Lundgren, T. S. & Mansour, N. N. 1988 Oscillations of drops in zero gravity with weak viscous effects. *J. Fluid Mech.* **194**, 479.

Marston, P. L. 1980 Shape oscillations and static deformation of drops and bubbles driven by modulated radiation stresses: theory. *J. Acoust. Soc. Am.* **67**, 15.

Marston, P. L. & Apfel, R. E. 1979 Acoustically forced shape oscillations of hydrocarbon drops levitated in water. *J. Colloid Interface Sci.* **68**, 280.

Marston, P. L. & Apfel, R. E. 1980 Quadrupole resonance of drops driven by modulated acoustic radiation pressure: experimental properties. *J. Acoust. Soc. Am.* **67**, 27.

Miller, C. A. & Scriven, L. E. 1968 The oscillations of a fluid droplet immersed in another fluid. *J. Fluid Mech.* **32**, 417.

Morse, P. M. 1948 *Vibration and Sound*. McGraw-Hill.

Pelekasis, N. A., Tsamopoulos, J. A. & Manolis, G. D. 1991 Nonlinear oscillations of liquid shells in zero gravity. *J. Fluid Mech.* **230**, 541.

Prosperetti, A. 1980 Normal-mode analysis for the oscillations of a viscous liquid drop in an immiscible liquid. *J. Méc.* **19**, 149.

Rayleigh, Lord 1879 On the capillary phenomena of jets. *Proc. R. Soc. Lond.* A **29**, 71.

Reid, W. H. 1960 The oscillations of a viscous liquid drop. *Q. Appl. Maths* **18**, 86.

Shi, T. & Apfel, R. E. 1995*a* Oscillations of a deformed liquid drop in an acoustic field. *Phys. Fluids* **7**, 1545.

Shi, T. & Apfel, R. E. 1995*b* Instability of a deformed liquid drop in an acoustic field. *Phys. Fluids* **7**, 2601.

Shi, W. T. & Apfel, R. E. 1996 Deformation and position of acoustically levitated drops. *J. Acoust. Soc. Am.* **99**, 1977.

Tian, Z., Holt, R. G. & Apfel, R. E. 1993 Deformation and location of acoustically levitated liquid drops. *J. Acoust. Soc. Am.* **93**, 3096.

Tikhonov, A. N. & Samarskii, A. A. 1990 *Equations of Mathematical Physics*. Dover.

Trinh, E. H. & Hsu, C.-J. 1986 Equilibrium shapes of acoustically levitated drops. *J. Acoust. Soc. Am.* **79**, 1335.

Trinh, E. & Wang, T. G. 1982 Large-amplitude free and driven drop-shape oscillations: experimental observations. *J. Fluid Mech.* **122**, 315.

Trinh, E., Zwern, A. & Wang, T. G. 1982 An experimental study of small-amplitude drop oscillations in immiscible liquid systems. *J. Fluid Mech.* **115**, 453.

Tsamopoulos, J. A. & Brown, R. A. 1983 Nonlinear oscillations of inviscid drops and bubbles. *J. Fluid Mech.* **127**, 519.